Electric Current Density and Temperature Field around Corner Crack at a Hole under Joule Heating

Thomas Jin-Chee LIU

Department of Mechanical Engineering, Ming Chi University of Technology
Taishan, New Taipei City, Taiwan
E-mail: jinchee@mail.mcut.edu.tw

ABSTRACT. *Using the coupled-field finite element method, this paper discusses the electric current density and temperature field around the corner crack at a hole in a metal plate under the electric load. As a result, the Joule heating effect causes a local hot point at the crack tip. This hot point can be applied on the crack detection or crack arrest. By varying the magnitude of the external current, the crack arrest or crack detection can be achieved.*

INTRODUCTION

When a cracked metal plate is subjected to an electric load, locally higher values of electric current density occur near crack tips. This phenomenon is analogous to stress concentration or singularity in solid mechanics. By the Joule heating effect, a higher temperature will be induced in those regions experiencing higher electric current densities. Additional thermal stresses and deformations are thus also induced. For this topic, many references have reported the research results [1-8]. In Fig. 1, typical distributions of the electric current density and temperature field near the crack tip are illustrated.

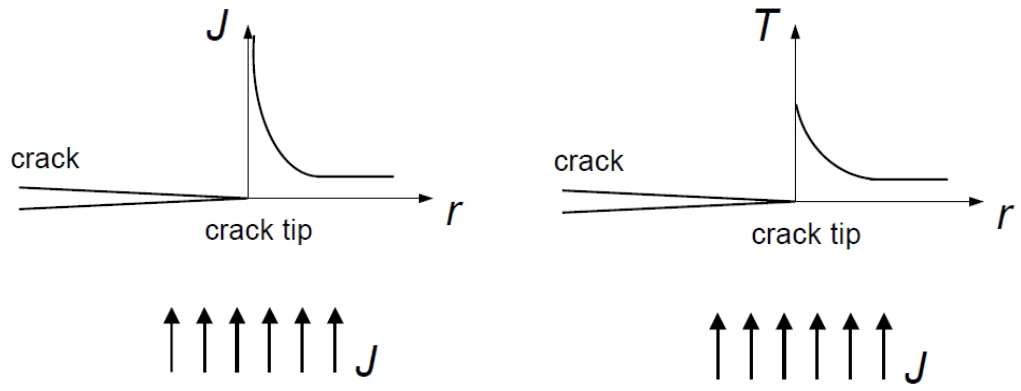

Figure 1. Distributions of electric current density (J) and temperature (T) near crack tip.

Similar to the stress concentration, the electric current density should have the same behavior around a hole. Furthermore, the electric and thermal problems of the corner crack at a hole are worth studying. Using the coupled-field finite element method, this paper discusses the electric current density and temperature field around the corner crack at a hole in a metal plate under the electric load. The practical and complicated results are obtained when the temperature-dependent material properties are adopted in the finite element analysis.

CASE STUDY

The case study of this paper is illustrated in Fig. 2. A metal plate with a central hole and a corner crack is subjected to a remote stress σ_0 and an electric current I_0. A constant value of I_0 is used to simulate the DC. This thin plate is made of mild steel with dimensions $W \times L$ and thickness e. The radius of the hole is R. The crack length is a.

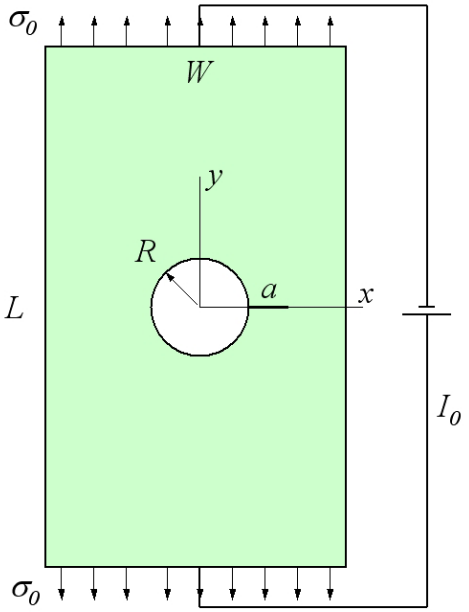

Figure 2. Case study of this paper.

The thermo-electro-structural coupled-field problem in Fig. 2 will be solved by the finite element method using the software ANSYS [9]. The two-dimensional conditions, plane stress assumption and isotropic properties are used. To simulate more practical conditions, the temperature-dependent material properties in Table 1 [10] are adopted in the analysis. The use of the temperature-independent material properties may lead to incorrect results. This issue will be discussed in this paper.

Under the Joule heating, the current-induced thermo-structural problem is transient. Contact conditions between both crack surfaces are considered in this study. The electric current and heat flow can pass through the crack surfaces when the crack contact occurs.

Table 1. Temperature-dependent properties of mild steel [10]

Temperature (°C)	Young's modulus E (GPa)	Yielding strength S_Y (MPa)	Coefficient of thermal expansion α (1/°C)	Thermal conductivity k (W/ m-°C)	Specific heat C_p (J/ kg-°C)	Resistivity ρ (Ω-m)
21	206.8	248	10.98×10^{-6}	64.60	444	0.14224×10^{-6}
93	196.5	238	11.52×10^{-6}	63.15	452.38	0.18644×10^{-6}
204	194.4	224	12.24×10^{-6}	55.24	511.02	0.26670×10^{-6}
315.5	186	200	12.96×10^{-6}	49.87	561.29	0.37592×10^{-6}
426.7	169	173	13.50×10^{-6}	44.79	611.55	0.49530×10^{-6}
537.8	117	145	14.04×10^{-6}	39.71	661.81	0.64770×10^{-6}
648.9	55	76	14.58×10^{-6}	34.86	762.34	0.81788×10^{-6}
760	6.9	14	14.05×10^{-6}	30.46	1005.3	1.0109×10^{-6}
871	–	–	13.05×10^{-6}	28.37	1005.3	1.1151×10^{-6}
982	–	–	–	27.62	1005.3	1.1582×10^{-6}
1093	–	–	–	28.52	1189.6	1.1786×10^{-6}
1204	–	–	–	–	1189.6	1.2090×10^{-6}

Poisson's ratio ν= 0.3, density β = 7861.2 kg/m^3, melting point = 1521 ºC.

METHODS OF ANALYSES

In this study, the finite element equations of the thermo-electro-structural coupled-field analysis are listed as follows [9]:

$$\begin{bmatrix} \mathbf{M} & 0 & 0 \\ 0 & 0 & 0 \\ 0 & 0 & 0 \end{bmatrix} \begin{bmatrix} \ddot{\mathbf{U}} \\ \ddot{\mathbf{T}} \\ \ddot{\mathbf{V}} \end{bmatrix} + \begin{bmatrix} \mathbf{C} & 0 & 0 \\ \mathbf{C}^{\mathbf{tu}} & \mathbf{C}^{\mathbf{t}} & 0 \\ 0 & 0 & 0 \end{bmatrix} \begin{bmatrix} \dot{\mathbf{U}} \\ \dot{\mathbf{T}} \\ \dot{\mathbf{V}} \end{bmatrix} + \begin{bmatrix} \mathbf{K} & \mathbf{K}^{\mathbf{ut}} & 0 \\ 0 & \mathbf{K}^{\mathbf{t}} & 0 \\ 0 & 0 & \mathbf{K}^{\mathbf{v}} \end{bmatrix} \begin{bmatrix} \mathbf{U} \\ \mathbf{T} \\ \mathbf{V} \end{bmatrix} = \begin{bmatrix} \mathbf{F} \\ \mathbf{Q} \\ \mathbf{I} \end{bmatrix} \tag{1}$$

where **U**, **T**, **V**, **F**, **Q** and **I** are the vector forms of the displacement, temperature, electric potential, force, heat flow rate and electric current, respectively. The material constant matrices **M**, **C**, $\mathbf{C}^{\mathbf{t}}$, $\mathbf{C}^{\mathbf{tu}}$, **K**, $\mathbf{K}^{\mathbf{t}}$, $\mathbf{K}^{\mathbf{ut}}$ and $\mathbf{K}^{\mathbf{v}}$ are the structural mass, structural damping, thermal specific heat, thermo-structural damping, structural stiffness, thermal conductivity, thermo-structural stiffness and electric conductivity, respectively. The coupled heat flow matrix **Q** contains the effects of the thermal loading and electrical Joule heating. $\mathbf{C}^{\mathbf{tu}}$ and $\mathbf{K}^{\mathbf{ut}}$ are thermo-structural coupled terms. Eq. (1) is a directly coupled nonlinear equation which is solved using the Newton-Raphson iterative method.

Referring to Fig. 2, the boundary and initial conditions are listed below:

$$J(x,-L/2,t) = J_0(t) \ , \ \phi(x,L/2,t) = 0 \ , \ |x| \le W/2 \tag{2}$$

$$\sigma_{yy}(x,L/2,t) = \sigma_{yy}(x,-L/2,t) = \sigma_0 \ , \ |x| \le W/2 \tag{3}$$

$$T(x,y,0) = T_0 = 25°C \tag{4}$$

$$u_i(x,y,0) = \dot{u}_i(x,y,0) = \ddot{u}_i(x,y,0) = 0 \tag{5}$$

where $J_0 = I_0/(eW)$. Due to the small time span (t < 1 s) of the electric load, all surfaces of the plate are assumed to undergo adiabatic processes [7].

On the crack surfaces ($R \le x \le R+a$, y=0), the electrical-thermal-mechanical contact conditions with numerical contact parameters will be considered in the simulations. The following equations describe the electrical and thermal contact conditions [10,11] :

$$J = \eta_{cel}(\phi_1 - \phi_2) \tag{6}$$

$$q'' = \eta_{cth}(T_1 - T_2) \tag{7}$$

where η_{cel} and η_{cth} are respectively the electrical conductance and thermal conductance of the contact surfaces. The terms $(\phi_1 - \phi_2)$ and $(T_1 - T_2)$ are respectively the electric potential difference and temperature difference between both contact surfaces.

Fig. 3 shows the finite element mesh of ANSYS with W=25 mm, L=200 mm, R=2 mm and a=2 mm. The plate thickness is e=0.1 mm. The plate is modeled by ANSYS element type: PLANE223, i.e. the 8-node isoparametric plane element with the thermo-electro-structural coupled-field analysis. The plane stress option is used due to the thin thickness. The nodal degrees-of-freedom of PLANE223 are u_x, u_y, T, and ϕ. In Fig. 3, the model has 2162 elements and 6620 nodes. The quarter-point elements (QPE) [12] are used for modeling the $r^{-1/2}$ singularity at the crack tip.

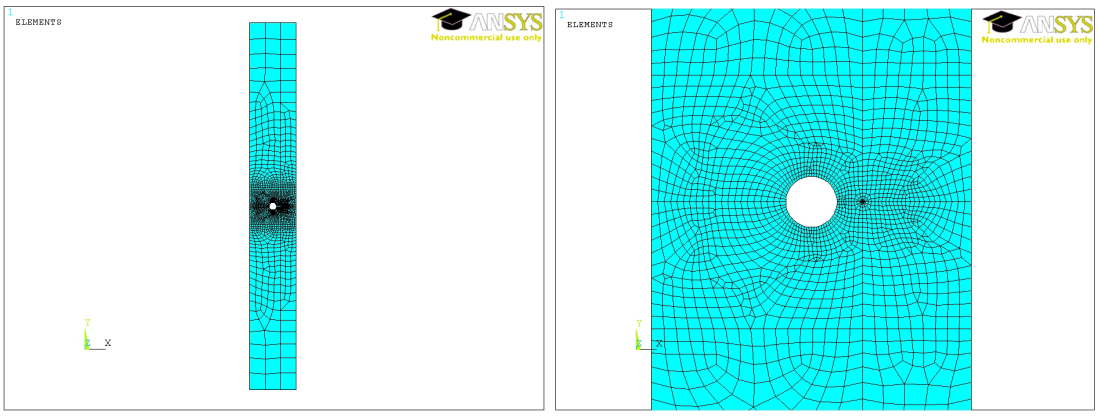

Figure 3. Finite element mesh.

RESULTS AND DISCUSSIONS

High Temperature Area around Hole and Crack Tip

The DC I_0=600 A is applied on the metal plate. The mechanical load is removed (σ_0=0 MPa). The temperature-dependent material data in Table 1 are adopted in the analysis. The elasto-plastic model with temperature-dependent properties is also used. For the plastic stress-strain region, the tangent modulus E_T is set as E_T =0.05E.

Fig. 4(a) shows the temperature contour at t=0.04 s. It can be seen that the Joule heating effect causes a high temperature area at the crack tip. Also, there is a local hot area near the hole. As a result in Fig. 4(b), it shows the electric current density vectors near the crack tip at t=0.04 s. It is noted that there are field concentrations near the hole edge and crack tip. Similar to the elastic stress field, the electric current density also has the $r^{-1/2}$ singularity at the crack tip [4].

The hot spot at the crack tip can be detected by the thermal sensor or infrared sensing system. The Joule heating effect helps us to detect the cracks or defects in the structures. This method is one kind of the non-destructive testing (NDT).

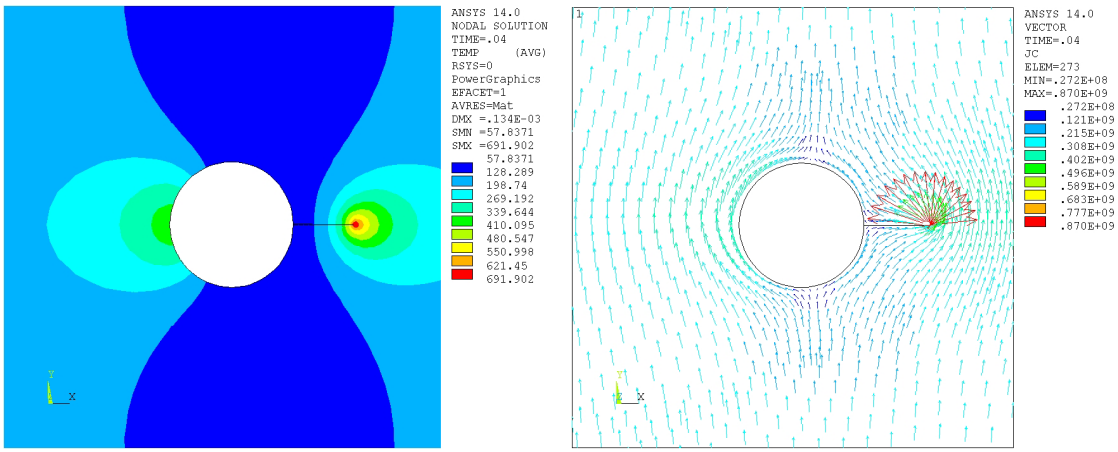

(a) (b)

Figure 4. (a) temperature contour (ºC); (b) electric current density vectors (A/m^2).

Temperature-Dependent Material Data

The numerical results from the temperature-dependent material data are compared with those from the temperature-independent material data. The later case uses the material data at 21°C in Table 1. In Fig. 5, it shows the effects of temperature-dependent material properties on the crack tip temperature under I_0=600 A. When the temperature-dependent material data are used, the results of the temperature are higher.

Temperature-dependent material data must be adopted in the analyses to obtain correct results. If constant (temperature-independent) material data are used, the results are incorrect and the temperatures are lower.

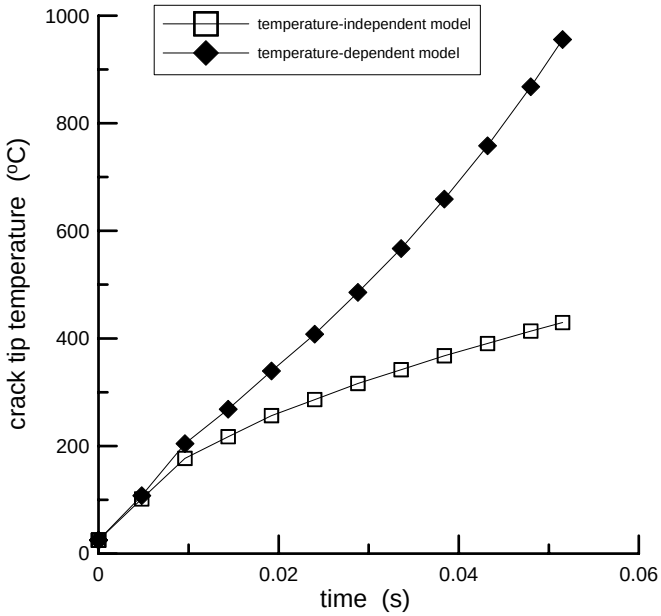

Figure 5. Effects of material data.

Elastic and Elasto-Plastic Models

As shown in Fig. 6, all stress-strain curves under different temperatures are used in the simulations. Also, the von Mises criterion and isotropic strain-hardening rule are used. However, the elasto-plastic strain and yielding zone may not have huge effects on the electric current density and temperature fields.

Fig. 7 shows the temperature results of the pure-elastic and elasto-plastic models. The difference between both curves is small when the temperature is high. To save the computation time or avoid non-linear divergence, the elastic model can be used.

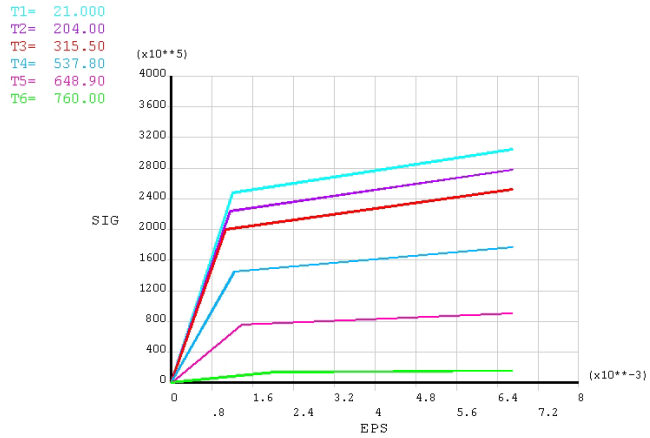

Figure 6. Stress-strain curves under different temperatures.

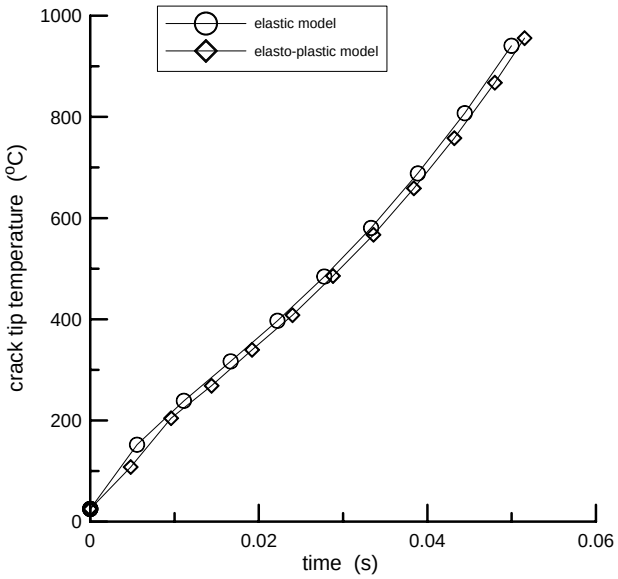

Figure 7. Effects of elasto-plastic model (I_0=600 A).

Effects of External Electric Current I_0

Fig. 8 shows the temperature distribution near the crack tip at t=0.0833 s. The temperature decreases from the crack tip to surrounding area. In Fig. 8(a), the result shows that it is easy to detect the hot spot at the crack tip under I_0=100 A. For detecting cracks in real mechanical or structural components, a measurement system including the thermal sensor and electric current supplier can be designed. The hot spot at the crack tip can be detected by the thermal sensor or infrared sensing system. Then the crack location can be determined.

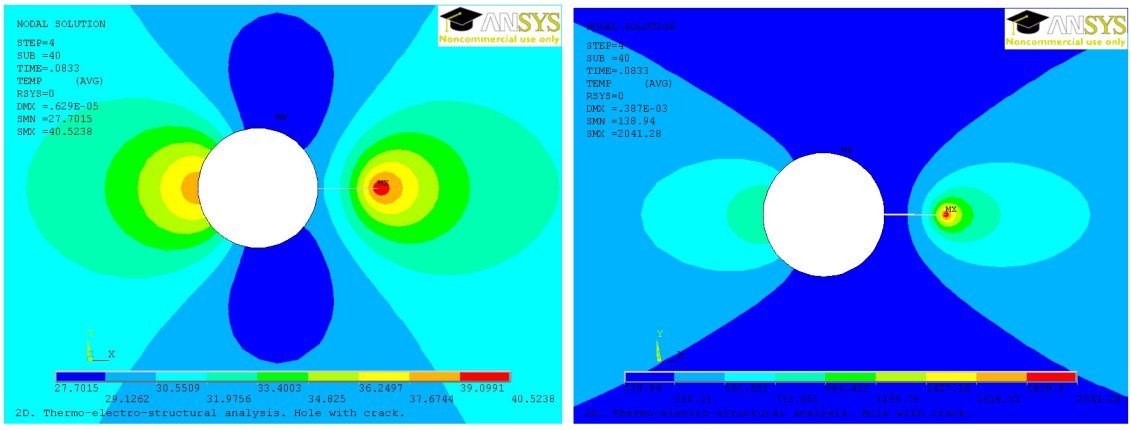

(a) (b)

Figure 8. Temperature field near crack tip. (a) I_0=100 A; (b) I_0=600 A.

In Fig. 8(b), the crack tip temperature is higher than the melting point (1521 ºC). The crack tip melts under high current I_0=600 A. In some experiments, it has been investigated that the crack tip can melt under high electric current loading and a crack tip hole occurs after the subsequent cooling process [5]. This hole, like a drilled hole, can reduce the stress concentration and remove the stress singularity at the crack tip. This way can prevent from the further crack growth.

CONCLUSIONS

Using the coupled-field finite element method, this paper has discussed the electric current density and temperature field around the corner crack at a hole in a metal plate under the electric load. The Joule heating effect causes a local hot point at the crack tip. This hot point can be applied on the crack detection or crack arrest. By varying the magnitude of the external current, the crack arrest or crack detection can be achieved.

Temperature-dependent material data must be adopted in the analyses to obtain correct results. If the temperature-independent material data are used, the results are incorrect. Also, to save the computation time or avoid non-linear divergence, the pure-elastic model can be used.

REFERENCES

1. Kudryavtsev, B.A., Parton, V.Z., Rubinskii, B.D. (1982) *Solids. Mech.* **17**, 110–118.
2. Parton, V.Z., Kudryavtsev, B.A. (1988) *Electromagnetoelasticity*, Gordon and Breach, New York.
3. Hasanyan, D., Librescu, L., Qin, Z., Young, R.D. (2005) *J. Therm. Stress* **28**, 729–745.
4. Cai, G.X., Yuan, F.G. (1999) *Int. J. Fract.* **96**, 279–301.
5. Fu, Y.M., Bai, X.Z., Qiao, G.Y., Hu, Y.D., Luan, J.Y. (2001) *Mater. Sci. Tech.* **17**, 1653–1656.
6. Liu, T.J.C. (2008) *Theor. Appl. Fract. Mech.* **49**, 171–184.
7. Liu, T.J.C. (2011) *Engng. Fract. Mech.* **78**, 666–684.
8. Liu, T.J.C. (2011) *Theor. Appl. Fract. Mech.* **56**, 154–161.
9. ANSYS, Inc. (2011) *ANSYS 14.0 Mechanical APDL Theory Reference*. SAS IP, Inc., USA.
10. Tsai, C.L., Dai, W.L., Dickinson, D.W., Papritan, J.C. (1991) *Weld J.* **70**, s339–351.
11. Sun, X., Dong, P. (2000) *Weld J.* **79**, s215–s221.
12. Barsoum, R.S. (1976) *Int. J. Numer. Meth. Eng.* **10**, 25–37.